Int. J. Electrochem. Sci., 16 **(2021)** Article Number: 211213, doi: 10.20964/2021.12.50

International Journal of
ELECTROCHEMICAL
SCIENCE
www.electrochemsci.org

A Novel State of Charge Estimation for Energy Storage Systems Based on the Joint NARX Network and Filter Algorithm

Huan Li, Chuanyun Zou[1,*], *Carlos Fernandez*[2], *Shunli Wang*[1], *Yongcun Fan*[1], *Donglei Liu*[1]

[1] School of Information Engineering, Southwest University of Science and Technology, Mianyang 621010, China;
[2] School of Pharmacy and Life Sciences, Robert Gordon University, Aberdeen AB10-7GJ, UK.
[*]E-mail: zouchuanyun@swust.edu.cn

Received: 8 August 2021 / *Accepted:* 17 September 2021 / *Published:* 10 November 2021

Lithium-ion batteries have the advantage of high energy density, low self-discharge rate, and long cycle life, and are currently the most widely used energy storage carriers. Accurate state of charge (SOC) estimation is essential to ensure the lithium-ion battery's safe and reliable operation. In order to improve the accuracy of estimation, this paper creatively applies the extended Kalman filter (EKF) to the improved nonlinear autoregressive algorithm with an exogenous neural network (NARXNN), forming a NARX-EKF neural network model for SOC prediction of the lithium-ion battery for the first time. This method avoids complicated equivalent modeling and parameter identification, rather directly maps the measured voltage, current, and temperature to the SOC. The data set is obtained by simulating the driving cycle load of the lithium-ion battery under different working conditions, and the network is tested under cyclic working conditions, dynamic working conditions, different temperature conditions, and different aging cycles. The SOC estimation results of the NARX-EKF model are evaluated from three aspects: mean absolute error (MAE), root mean square error (RMSE), and SOC error. Under cyclic conditions, the RMSE and MAE of NARXNN are only 1.4% and 1.3%, which is only 50% of other neural networks. In the dynamic working condition test, the maximum error of NARXNN optimized by EKF is reduced by about 50%, and the RMSE and MAE of the model are only 20% of other neural networks. When the ambient temperature changes, the RMSE and MAE of the model under low-temperature conditions were 1.2% and 0.9% respectively. The RMSE and MAE of the model under high-temperature conditions were 0.6% and 0.5% respectively. In addition, the NARX-EKF network can well solve the impact of different aging degrees of lithium-ion batteries on SOC estimation. When the battery health status is only 70%, the RMSE and MAE of the model were only 2.7% and 2.5% respectively. The results show that the NARX-EKF model has high accuracy, robustness, and good application prospects.

Keywords: Lithium-ion Battery; Nonlinear Autoregressive Neural Network; State-of-Charge; Extended Kalman Filter

1. INTRODUCTION

With the continuous development of new energy vehicles, large-scale energy storage, unique robots, and aerospace equipment, various batteries have been developed in recent years [1, 2, 3]. Compared with other batteries, lithium-ion batteries have the advantages of high energy density, low self-discharge rate, and long cycle life and are widely used in electric vehicles and other fields [4, 5, 6]. However, its online monitoring and security management still faces many challenges. An advanced, efficient, and real-time battery management system (BMS) is urgently needed to ensure its safe operation. Estimating the state of charge (SOC) of the battery is one of the main tasks of the BMS, which mainly affects the charging control, balance adjustment, and safety management of the BMS [7, 8, 9].

The SOC of the battery is an essential indicator for evaluating the available energy of the electric vehicle battery. Due to the complex structure and complicated working conditions of the lithium-ion battery [10, 11], the lithium-ion battery has uncertain characteristics such as nonlinearity and time-varying. Therefore, it is tough to directly calculate the SOC of the battery [12, 13, 14]. To solve this problem, many researchers in the world have conducted a lot of research and for nonlinear problems, the main idea is to linearize the system through equivalent circuit modeling or treat the system as a black box model through machine learning algorithms. In order to solve the time-varying problem, the main technique is to use time series to iterate the system and update the time continuously. The first approach is the current integration method [15, 16, 17, 18, 19]. The second approach is through EKF [20, 21, 22], PSO [23, 24, 25, 26] and UKF [11, 27] represent the recursive algorithm. The third approach is to use machine learning algorithms represented by support vector machines, decision trees, and neural networks [28, 29].

For the SOC estimation of lithium batteries, the current integration method is currently most commonly used and in SOC estimation, its application history is much longer than other methods. This is because of its admirable simplicity and the fact that you can ignore the battery's internal structure and external circuit characteristics. However, this method estimates SOC in an open loop, and the error accumulates over time. Therefore, constant recalibration is required and with the times change, simple current integration methods can no longer meet our requirements for accuracy. Since a load of an electric vehicle is dynamic, it will inevitably cause noise interference to the current and terminal voltage of the battery. Due to the above problems, the Kalman filter recursive algorithm based on the equivalent circuit model can greatly improve the noise problem and is widely used in the SOC estimation of single cells and battery packs. For the SOC estimation method of battery packs, most scholars treat the battery pack as a single large battery through equivalent modeling. Due to the nonlinear characteristics of SOC, EKF [30, 31] have been widely adopted. [32] established the BCM of 120 LFP series batteries, adopted the second-order RC model to represent the whole pack, and used the improved EKF algorithm to implement the battery SOC estimation. [33] employed EKF to identify MCM parameters online and used the Unscented Kalman filter to estimate the SOC of each cell of the battery pack. Although recursive algorithms such as Kalman filtering are widely used, the uncertainty in the calculation process of the recursive algorithm may accumulate, leading to system instability or divergence. In addition, the calculation time of these two algorithms may be much longer than other methods [34, 35, 36, 37].

With the continuous improvement of computer computing power and big data science and technology, modern machine learning technology is progressing faster than ever. Scholars from all walks of life have studied artificial intelligence algorithms in recent years and applied them in their research. Artificial Neural Network (ANN) is a computational model based on the structure and function of biological neural networks and is a widely used artificial intelligence algorithm. The artificial neural network is self-adaptive and can adjust well to the battery performance of the nonlinear system. Most of the ANN-based SOC estimation algorithms use traditional multi-layer perceptrons, which are trained through backpropagation. This article will introduce NARXNN for SOC estimation, a dynamic neural network with a feedback unit and a recursive neural network. The structure is composed of two parts: a feedforward neural network and an output feedback neural network. The network structure adds a delay feedback unit to reuse the output feedback. Concerning memory function, NARXNN has a relatively strong learning ability, and time series prediction performance is better than ordinary neural networks. The voltage, current, and SOC data of the battery during use are time-varying time series, so NARXNN is very suitable for battery systems. This article mainly includes the following innovations: (1) To improve the performance of NARXNN further, the network output results are optimized through EKF, which significantly reduces the random error caused by dynamic changes in working conditions and enhances the stability of the network structure. (2) The NARX-EKF model directly maps the voltage, current and temperature of the lithium-ion battery to the SOC without complicated processing. (3) The NARX-EKF model was trained and tested under different temperatures and complex working conditions to ensure that the model is suitable for different driving conditions. (4) The model is tested under different aging cycles to ensure that it can solve the impact of different degrees of aging of lithium-ion batteries on SOC estimation.

2. MATHEMATICAL ANALYSIS

Artificial Neural Network (ANN) is a mathematical tool with a multi-layer network structure [38, 39]. Each layer contains many processing units called "neurons" as fundamental units [40]. Due to its large number of parallel structures, it has high stability and robustness [41]. The ANN-based NARXNN method has improved learning performance and fast calculation speed and is suitable for solving the nonlinear characteristics of lithium-ion batteries [42].

2.1. NARX neural network

The NARXNN mainly includes four parts: input delay layer, output delay layer, hidden layer, and output layer. As shown in Fig. 1. It can be seen from the structure diagram of NARXNN that after the input vector and the output vector are weighted and added, they are input into the hidden layer. The hidden layer has data from the input and output delay layers and thresholds to calculate. Then, the data of the hidden layer is processed by the function $f_h(\cdot)$ as the output layer's input data, the output layer and the hidden layer also have an output layer threshold. The output data of the hidden layer is multiplied by the adjustable weight and then added to the threshold, and then calculated by the function $f_0(\cdot)$. The function expression of the neural network is shown in formula (1):

$$y(n+1) = f[y(n-d_y),\cdots,y(n-1);x(n-d_u),\cdots,x(n-1),x(n)] \quad (1)$$

As mentioned in the above formula, where $f(\cdot)$ is the nonlinear function of the neural network, $x(n)$ is the network input vector, $y(n)$ is the network output vector, d_y is the output delay coefficient, and d_u is the input delay coefficient.

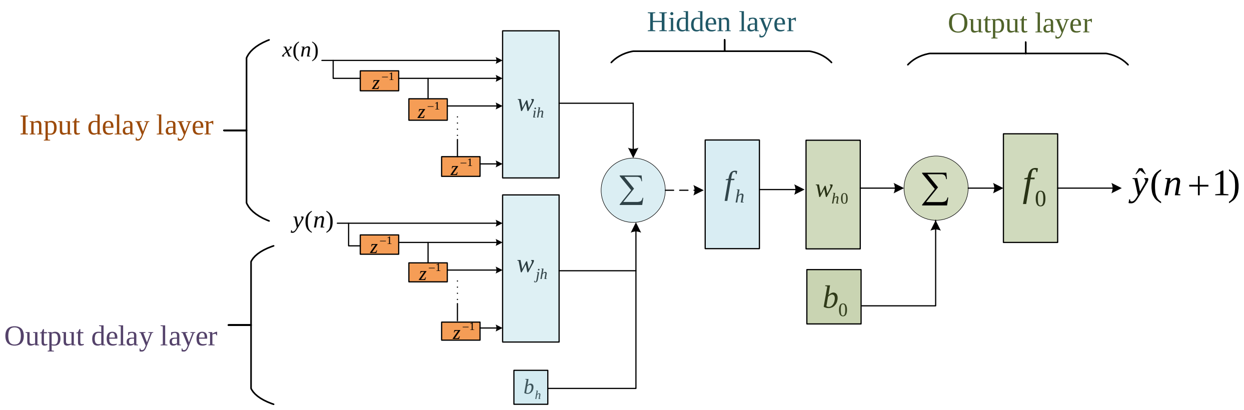

Figure 1. NARX network structure

The core structure of NARXNN is the delay feedback unit. From the function expression of the neural network, it can be seen that the output of the model at the current time is not only related to the input value at the previous time but also related to the previous output values. The output data passes through the delay feedback unit and the step size of the output feedback is determined by the size of d_y. The feedback of the output data can improve the convergence speed of the model and the accuracy of the prediction.

The NARXNN contains two different structures, as shown in Figure 2, (a) is the structure diagram of the open-loop network, (b) is the structure diagram of the closed-loop network. In the open-loop structure, the input and output sequences are known. The real target value is directly input into the delay feedback unit to calculate and predict the output value at the next moment. Since the input of the output feedback delay unit is a real value, the recursive accumulation of errors is avoided. This mode does not have a feedback unit, which will make the network model forward, and the network will converge faster and have a higher accuracy during training. In the closed-loop structure, the input signal of the delayed feedback unit is the output of the NARXNN at the last time. This mode is used when the target variable is unknown, and the input of the feedback layer is the predicted value of the neural network at the last time. The NARX network structure is as shown in Fig. 2.

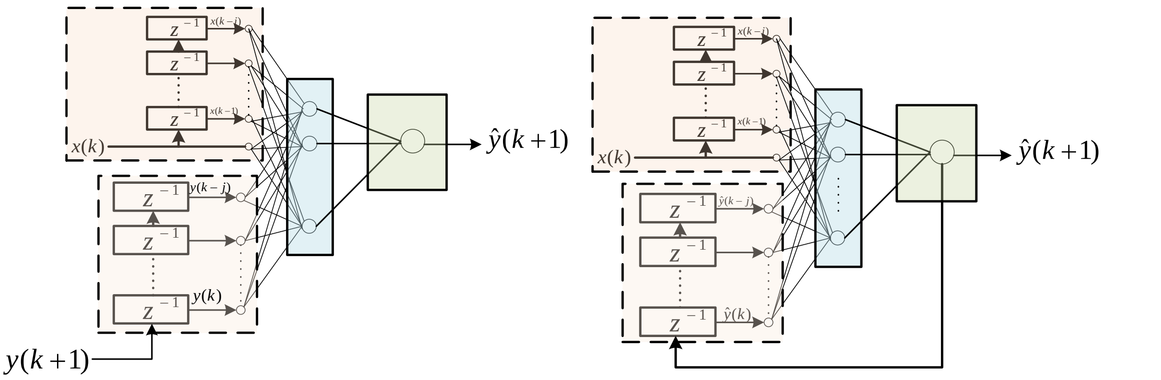

(a) Open-loop network (b) Closed-loop network

Figure 2. NARX network structure in two modes

In the process of predicting the battery SOC, the three variables, voltage, current, and temperature can be directly measured by different sensors so that they can be used as the input of the neural network, and the target is the value of the SOC at each moment. To evaluate the performance of the NARXNN in estimating SOC, this study conducted SOC estimation in two modes, compared and analyzed, and summarize the working conditions of the two modes.

2.2. NARX-EKF network

The essence of the Kalman filter is a series of mathematical calculation equations to realize functions such as prediction and correction. An optimal estimation algorithm and the extended Kalman filter (EKF) are a kind of Kalman filter. Since the NARXNN lacks stability in the SOC estimation of the charging and discharging process under complex conditions, this study will use the extended Kalman filter to improve the NARXNN model to optimize the estimation performance of the network model. The NARX-EKF model is shown in Fig. 3.

Generally, the Kalman filter estimation method usually uses the equivalent circuit model to establish the observation equation. The ampere-hour integration process gives the discrete state-space equation of the system. In this study, the NARXNN model is equivalent to the observation equation. The SOC value estimated by the NARXNN is input into the EKF module for filtering, thereby eliminating noise and random errors and further optimizing the SOC estimation. Equations (2) and (3) are the state equation and measurement equation of EKF, respectively.

$$SOC_{k+1} = SOC_k - \left(\frac{\eta \Delta t}{Q_N}\right) i_k + w_k \tag{2}$$

$$E_k = SOC_k + v_k \tag{3}$$

In the above equations, i_k is the current value at time k, SOC_k is the estimated value of the SOC state at time k, η is the charge and discharge efficiency, Q_N is the rated battery capacity, w_k and v_k are process noise and measurement noise, E_k is the estimated value of the NARXNN at time *k*. The Jacobian matrix is obtained by using Taylor series expansion to linearize the state space equation. A more accurate result can be obtained in a nonlinear dynamic system than the primary Kalman filter, thereby reducing the cumulative error of the open-circuit voltage.

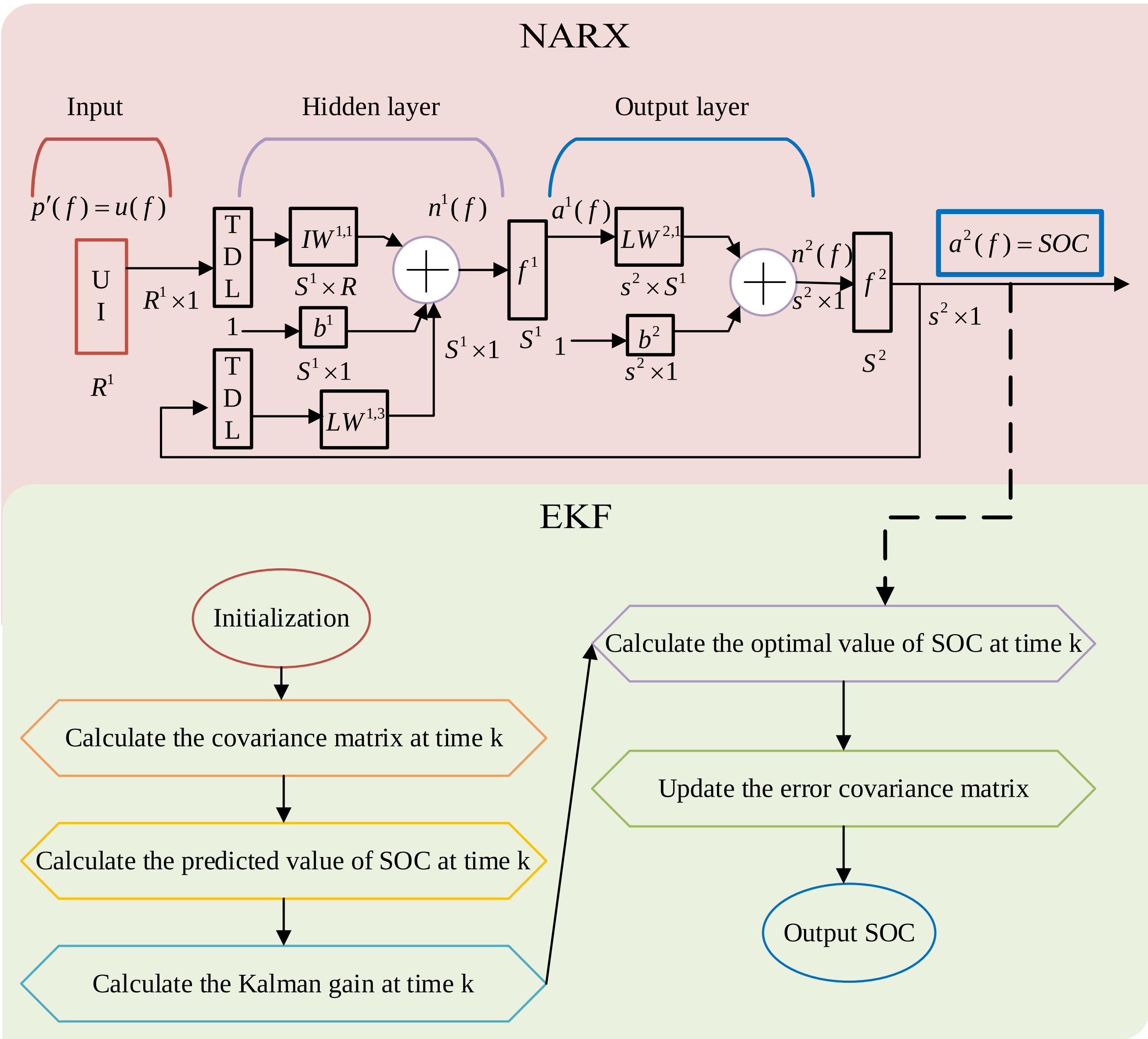

Figure 3. NARX-EKF network structure

The Kalman filter method after the extended application is called the extended Kalman filter algorithm. The recursive steps of EKF are shown in Table 1.

Table 1. EKF algorithm steps

Step	Algorithm	Operation
1	Initialization	$x_{0\|0}, p_{0\|0}$
2	State prediction	$x(k\|k-1) = A_{k-1}x(k-1) + B_{k-1}i_{k-1}$
3	Covariance prediction	$P(k\|k-1) = A_{k-1}\hat{P}_{k-1}A_{k-1}^T + Q_k$
4	Calculate Kalman gain	$K_k = P_k C_k^T \left(C_k P_k C_k^T + R_k\right)^{-1}$
5	State update	$\hat{x}_k = x(k\|k-1) + K_k\left[U_L(k) - C_k x(k\|k-1)\right]$
6	Noise covariance update	$\hat{P}_k = \left(E - K_k C_k\right)P_k$

As shown in the above table, $x_{0|0}$ represents the initial value of the state quantity, $p_{0|0}$ represents the initial value of the state error covariance, $x(k|k-1)$ represents the one-step prediction value of the state, i_{k-1} is the input of the system at k-1, which is the current at k in the SOC estimation, and A_{k-1} and B_{k-1} are the state transition matrix at k-1, $P(k|k-1)$ and $\hat{P}_{k-1}$ are the predicted value and estimated value of the state error covariance matrix, respectively. K_k and C_k are the Kalman gain value and state conversion matrix at time k, Q, And R represent the variance value of process noise and observation noise respectively. The noise value is difficult to determine and therefore, usually, it is enough to keep debugging to achieve the best algorithm. R and Q in this article are 0.1 and 0.001, respectively. $U_L(k)$ represents the system observation value at time k, that is, the SOC value output by NARX.

3. EXPERIMENTAL ANALYSIS

In order to verify the feasibility of the NARXNN in lithium-ion battery SOC estimation, an accurate lithium-ion battery SOC estimation model was constructed. The estimation accuracy and convergence of the model are verified under various experimental conditions. In this study, the ternary lithium-ion battery placed in the high and low temperature test box was tested using a power cell high-rate charge-discharge tester. The experimental platform is shown in Fig. 4. To simulate the complex EV battery load behaviour, the test object needs to perform a DST test, BBDST test, cyclic charge and discharge test, and different cycles of aging tests.

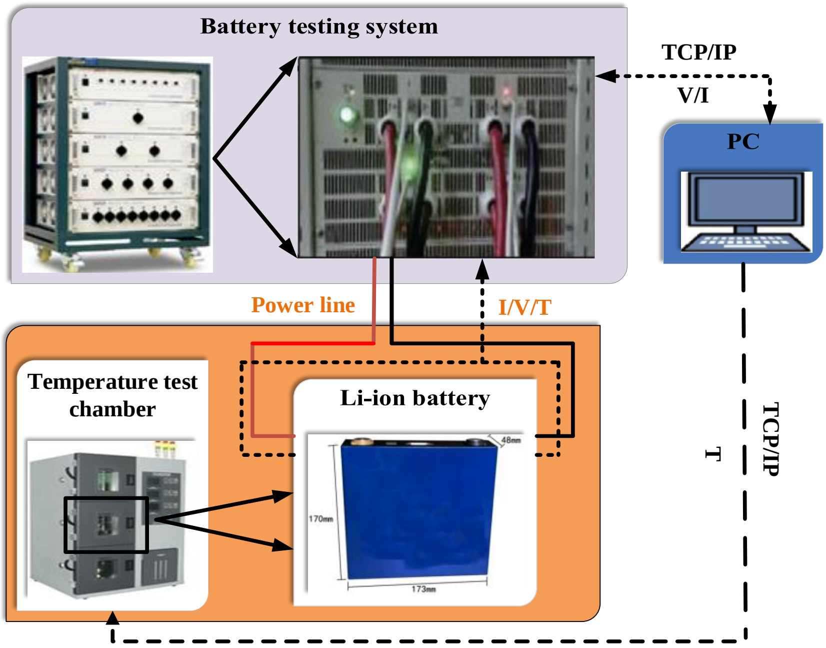

Figure 4. Experimental test platform

3.1. Analysis of cyclic charging and discharging conditions

The cyclic charging and discharging condition of the lithium-ion battery is the aging life test of the battery. To explore the accuracy of the SOC estimation of the NARXNN under the cyclic condition, the ambient temperature is set to 25 degrees. The data set is obtained by charging and discharging the battery for 100 cycles of constant voltage and constant current. The working condition data curve is shown in Fig. 5.

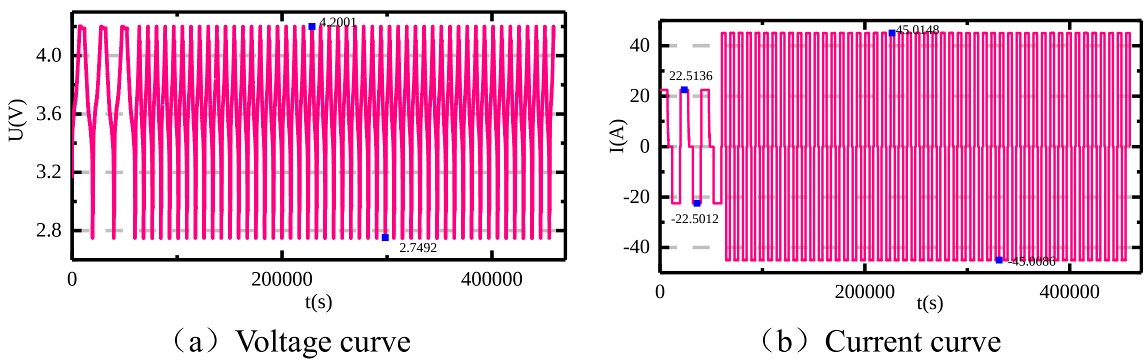

Figure 5. Data curve of cyclic charging and discharging conditions

As shown in the figure above, (a) is the voltage curve, and (b) is the current curve. To avoid overcharging or over-discharging the battery, the entire cycle of charge and discharge is performed within a safe threshold. In this experiment, 70% of the dataset was used for open-loop NARXNN training, and closed-loop NARXNN verified the remaining 30% of the data. The detailed program flow chart is shown in Fig. 6.

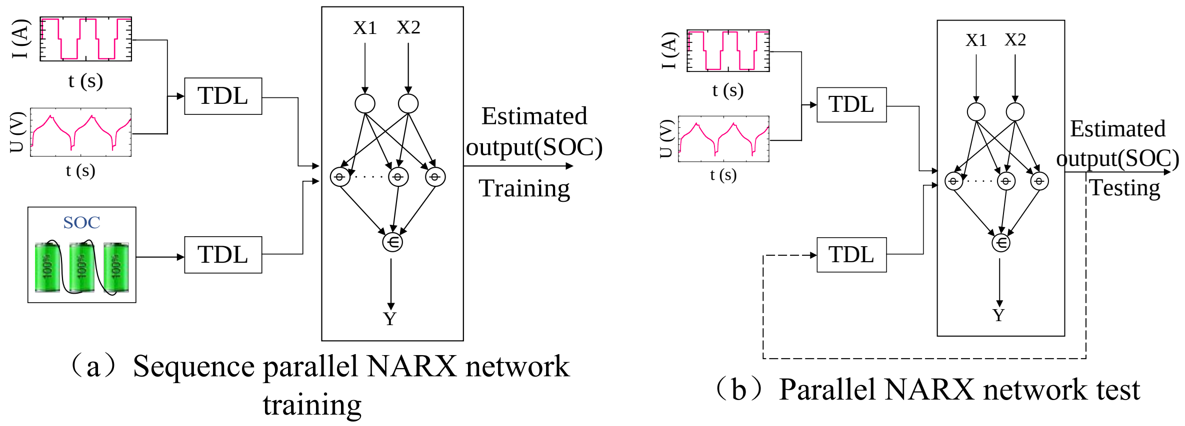

Figure 6. Cycle charge and discharge condition training test flow chart

As shown in the figure above, (a) is the sequence open-loop NARXNN training process. In the training process, current, voltage, and SOC are used as input variables, the SOC fitted by current integral is used as the target of network training, and the training output is SOC.

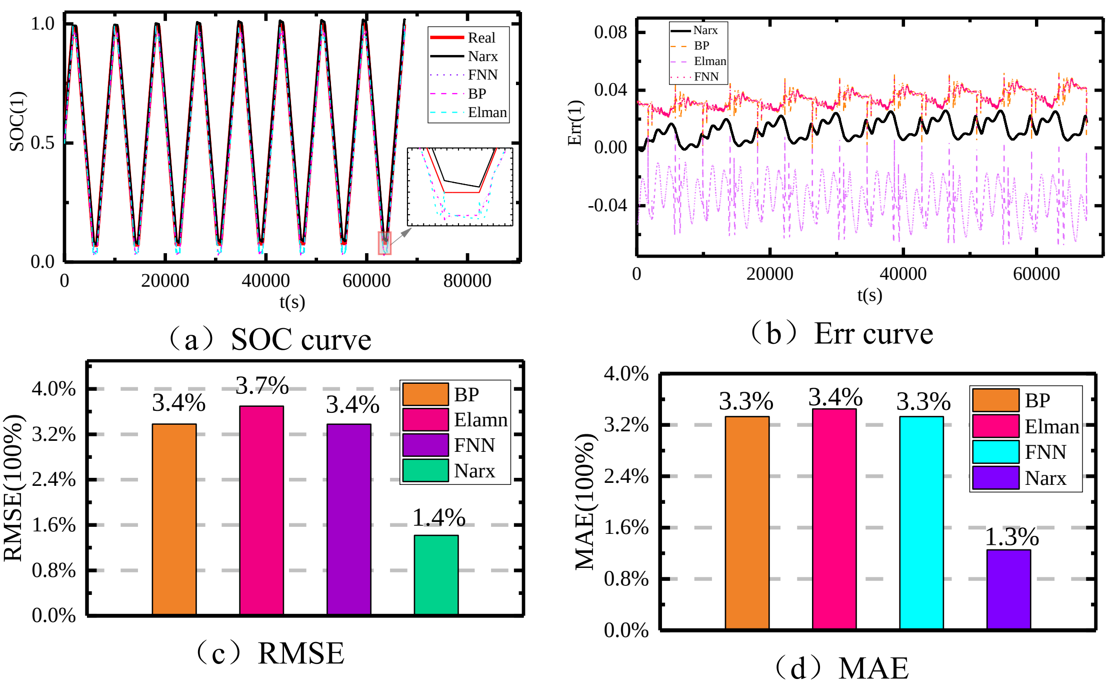

Figure 7. Estimation and simulation of cyclic charging and discharging conditions.

There is no feedback structure in the network, which greatly saves training time. (b) shows the closed-loop NARXNN test process. During the test, the feedback structure is added, and the training target is removed. Current and voltage are obtained as output to acquire SOC under the action of network mapping. The simulation result of the cyclic charging and discharging conditions are shown in Fig. 7.

As shown in the figure above, (a) is the SOC simulation diagram, (b) is the error curve diagram, (c) and (d) are the comparison diagrams of RMSE and MAE respectively. It can be observed that NARXNN has a good response and robustness in the test of cyclic working conditions and can accurately estimate the constantly changing SOC. From (b), (c), and (d), it can be seen that the maximum error of NARXNN is about 2.5%, which is smaller than other neural networks, and RMSE and MAE are only 1.4% and 1.3% respectively, which are much lower than other neural networks. In terms of calculation cost, the time spent by BPNN, FNN, and NARXNN is the same, about 30s. However, the ElmanNN needs more time.

3.2. Dynamic operating condition analysis

Through open-loop network training and closed-loop network testing, the improved algorithm has the characteristics of high accuracy and low delay, but this method is suitable for uncomplicated cycle conditions. In order to further verify the applicability of NARXNN, the closed-loop NARXNN is used for training and testing. On this basis, the complexity of the working conditions is increased. The dynamic working condition dataset is shown in Fig. 8.

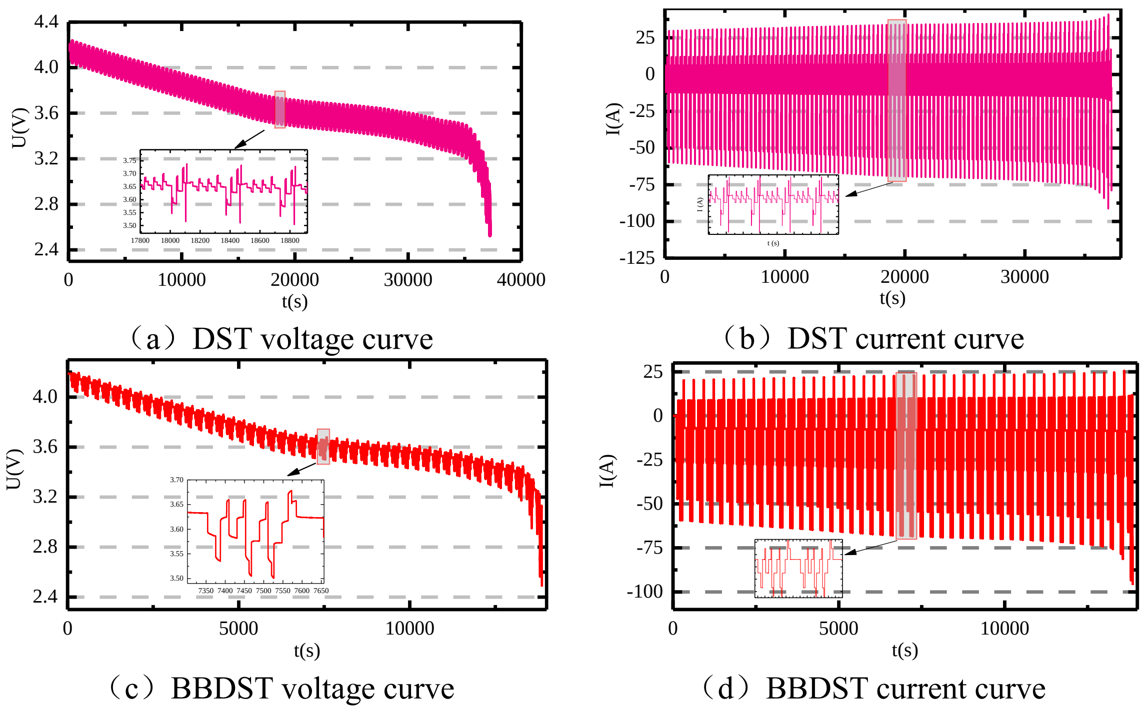

Figure 8. Dynamic working condition data set

Considering that the battery is running under dynamic working conditions in the actual application environment, to verify the effect and accuracy of the NARXNN algorithm following complex working conditions, the DST working condition data is used as the training set, and the BBDST working condition data is used as the test set. As shown in the above figure, (a) is the voltage under DST working condition, and (b) is the current under DST working condition, both of which are the input variables of the training set. (c) and (d) are BBDST operational condition data used as input variables of the test set. The algorithm simulation is shown in Fig. 9.

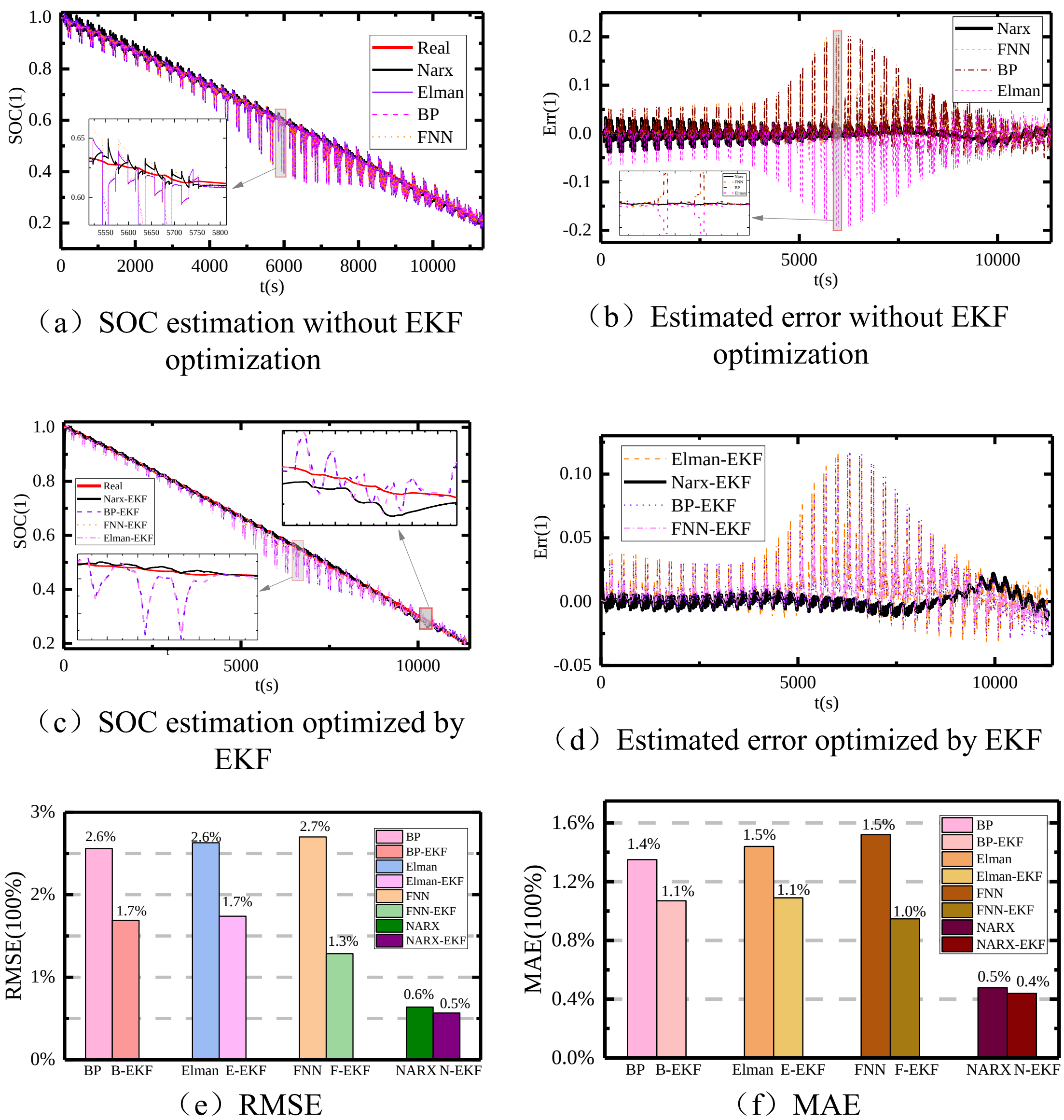

（a）SOC estimation without EKF optimization

（b）Estimated error without EKF optimization

（c）SOC estimation optimized by EKF

（d）Estimated error optimized by EKF

（e）RMSE

（f）MAE

Figure 9. Dynamic operating conditions test.

As shown in Fig. 9 (a) and (b), other neural networks except NARXNN have a considerable divergence during the estimation process. The NARXNN can follow the reference value steadily. The error is always less than 4%, which is much lower than other neural networks. Due to the rapid dynamic changes of the working conditions, the maximum value of the algorithm error often occurs when the voltage suddenly rises or falls, and the extreme change of data causes the network structure to be unstable. To suppress the noise caused by the data mutation, the EKF is added to reduce the tip error. (c) and (d) show that the various algorithms optimized by EKF have significantly reduced the tip error, and the maximum error has been reduced by about 50%. It can be seen more intuitively from (e) and (f) that the RMSE and MAE of NARXNN are only 20% of other neural networks, proving the superiority of the NARXNN. Compared with deep neural networks[43], the model proposed in this research has greater advantages. After EKF optimization, the error of each neural network is significantly reduced, which dramatically improves the estimation accuracy of the algorithm. This shows that EKF can effectively maintain the stability of the network and improve the estimation accuracy of the network. In terms of calculation cost, as the amount of data and the complexity of working conditions increase, to obtain the best estimation effect, the training time of each neural network has to be increased relative to simple working conditions. NARXNN, FNN, BPNN take about 90s to optimize, but ElmanNN takes more time.

3.3. Narrow temperature change test

Temperature is a critical parameter that affects SOC estimation. Seasonal changes, day and night changes, and heat generated during charging and discharging will all affect the surface temperature of the battery. To explore the impact of ambient temperature changes on the neural network's estimation performance, the network will be trained using the BBDST working condition data when the ambient temperature is 25°C, and the tests will be performed at the ambient temperature of 15°C and 35°C. Fig. 10 shows the simulation of the algorithm narrow temperature change test.

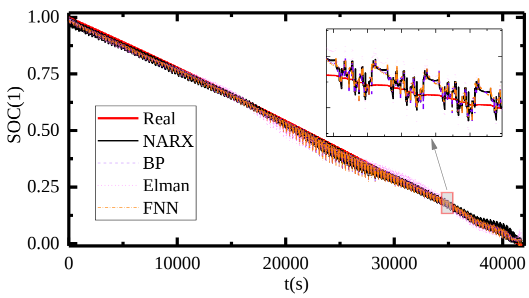

（a1）SOC estimation without EKF optimization

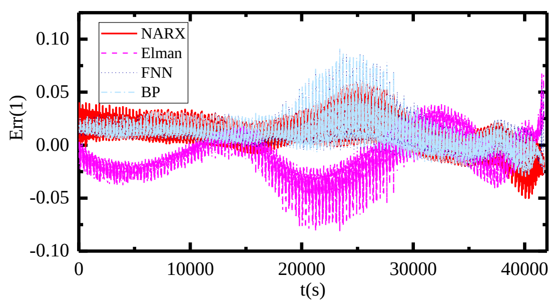

（a2）Estimated error without EKF optimization

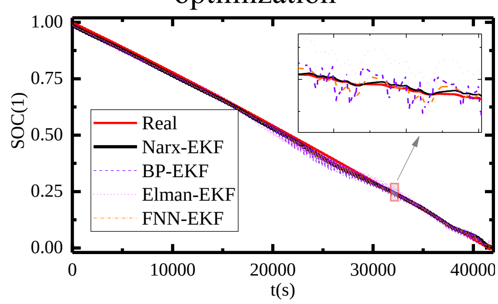

（a3）SOC estimation optimized by EKF

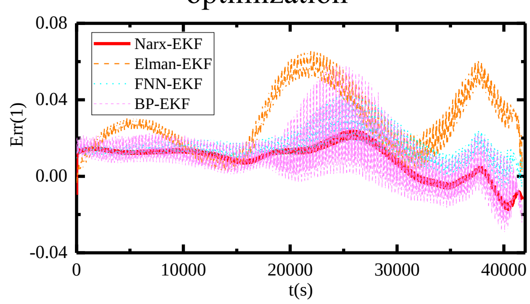

（a4）Estimated error optimized by EKF

(a) Test simulation when the ambient temperature is 15°C

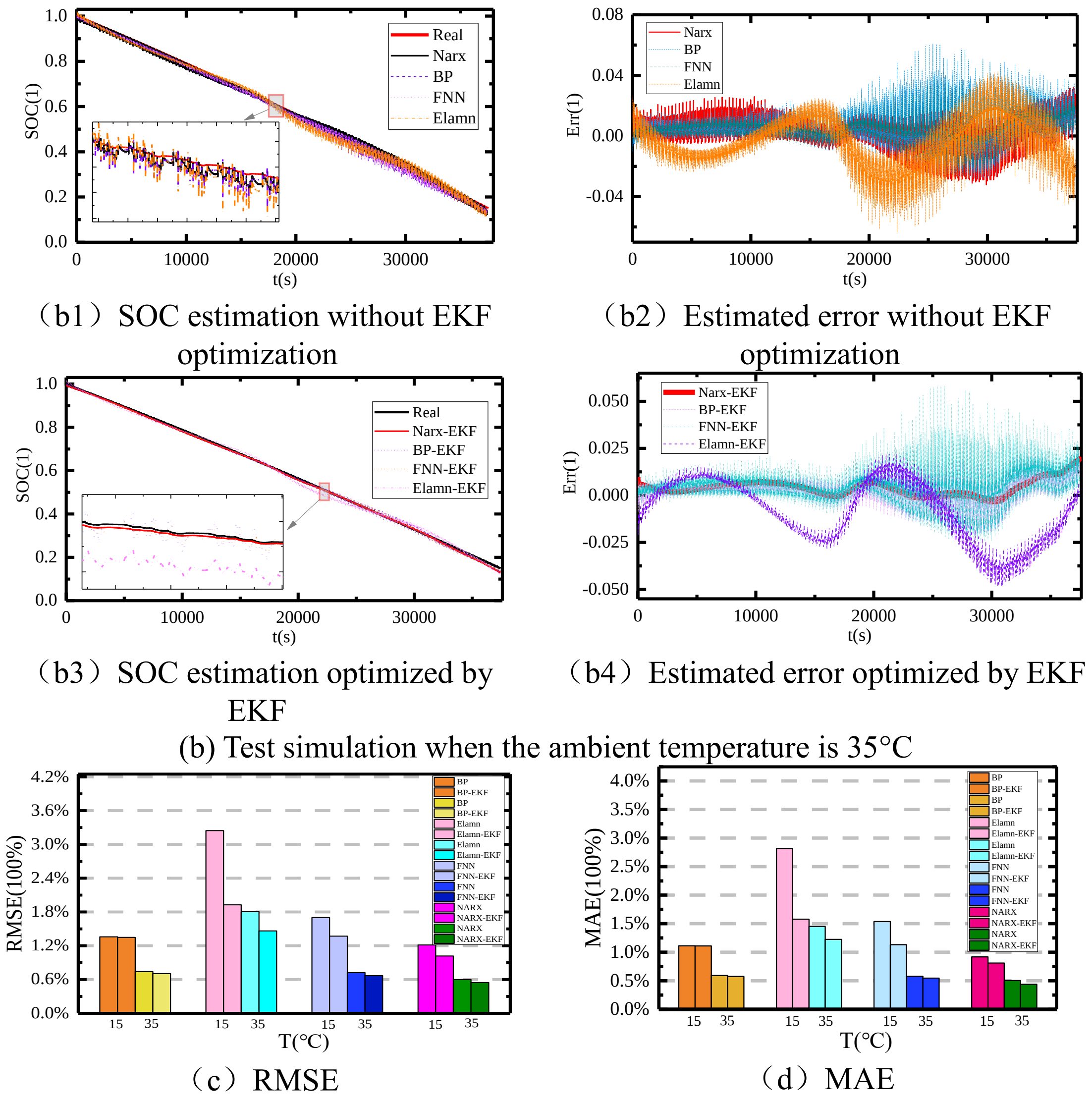

（b1）SOC estimation without EKF optimization

（b2）Estimated error without EKF optimization

（b3）SOC estimation optimized by EKF

（b4）Estimated error optimized by EKF

(b) Test simulation when the ambient temperature is 35°C

（c）RMSE

（d）MAE

Figure 10. Narrow temperature change test simulation.

(a) and (b) show that the NARXNN can smoothly follow the change of the reference value at low temperature and high temperature. The error is maintained within 4%, and the maximum error is much smaller than other neural networks. This verifies the accuracy of the NARXNN 's SOC estimation under temperature changes. After optimization by the EKF algorithm, the error of each neural network algorithm is significantly reduced, which substantially reduces the cutting-edge errors caused by drastic changes in data. (c) and (d) show the estimation advantage of the NARXNN. Under low-temperature conditions, the RMSE and MAE are 1.2% and 0.9%, respectively, and under high-temperature conditions, their RMSE and MAE are 0.6% and 0.5%, respectively. After EKF optimization, both errors are significantly reduced regardless of high temperature or low-temperature conditions. In addition, compared with RBF neural network, the model proposed in this research has greater advantages. The performance of DBF was promising with respect to achieving low estimation error with RMSE, MAE, and highest SOC error below 0.7%, 0.6%, and 5%, respectively under the DST drive cycle.[27] It can be seen that the NARX-EKF network can well solve the impact of narrow temperature changes on SOC estimation.

3.4. SOC estimation under different aging cycles

For unaged lithium-ion batteries, an excellent SOC estimation effect can be achieved through the NARX-EKF network and after hundreds of cycles, the internal characterization parameters of lithium-ion batteries change. Therefore, under different aging cycles, the accuracy and robustness of the proposed method are evaluated. As shown in Fig. 11, the capacity degradation performance of the (LiNCA) battery was evaluated under the four milestone aging cycles (42, 84, 126, and 168 cycles).

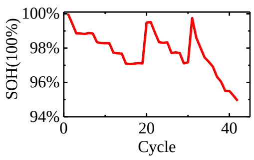

(a) SOH change after 42 aging cycles

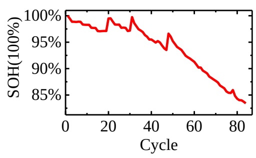

(b) SOH change after 84 aging cycles

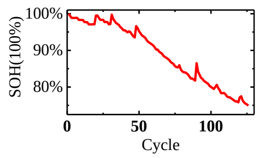

（c）SOH change after 126 aging cycles

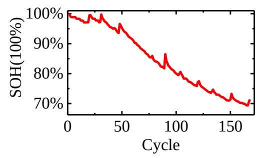

(d) SOH change after 168 aging cycles

Figure 11. SOH change under different aging cycles

As shown in the figure above, after 168 aging cycles, the battery's state of health (SOH) is 70%, 25% lower than the value after 42 aging cycles. This experiment uses the constant current discharge experiment dataset of unaged LiNCA batteries to train the algorithm and uses the dataset of 42, 84, 126, and 168 cycles of aging LiNCA batteries to test the performance of the trained model. The test result is shown in Fig. 12.

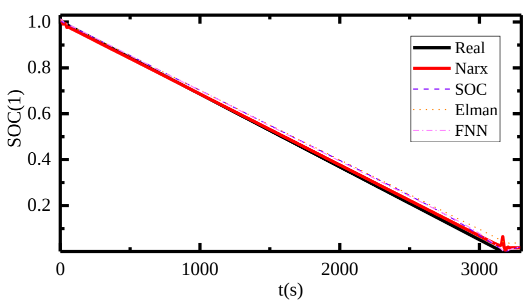

（a1）SOC estimation without EKF optimization

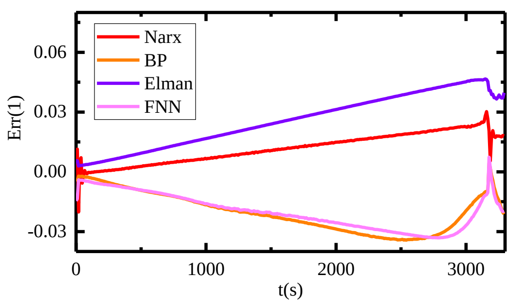

(a2) Estimated error without EKF optimization

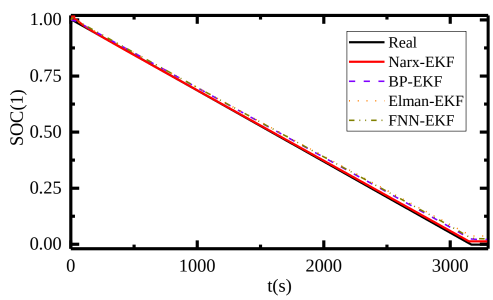

(a3) SOC estimation optimized by EKF

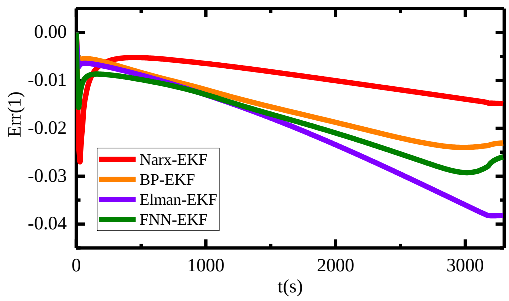

(a4) Estimated error optimized by EKF

(a) 42 aging cycles

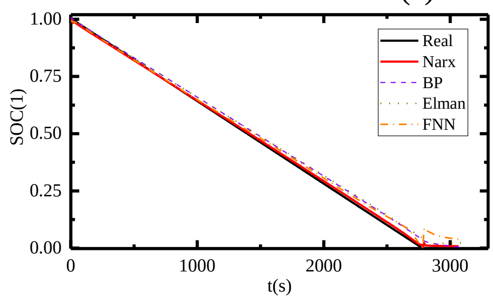

（b1） SOC estimation without EKF optimization

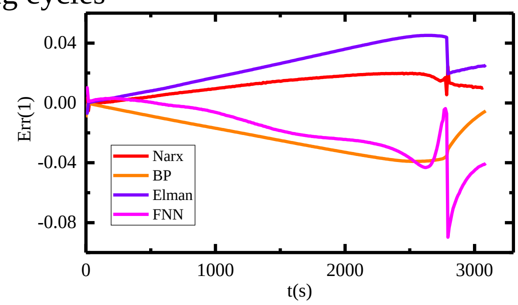

(b2) Estimated error without EKF optimization

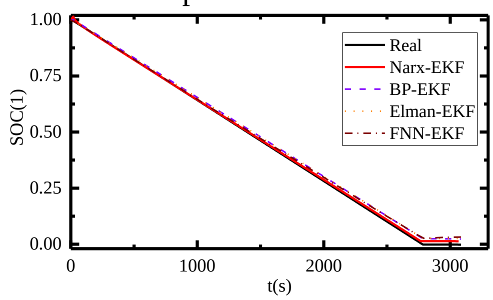

(b3) SOC estimation optimized by EKF

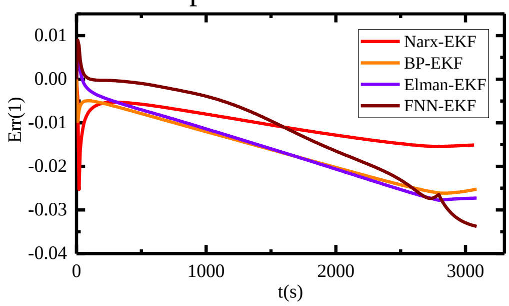

(b4) Estimated error optimized by EKF

(b) 84 aging cycles

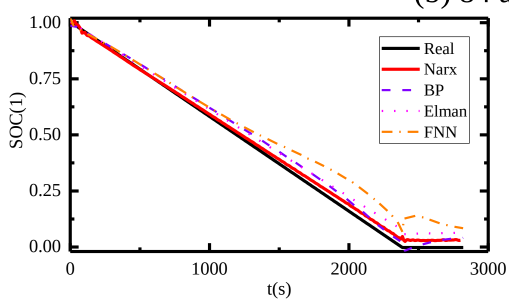

（c1） SOC estimation without EKF optimization

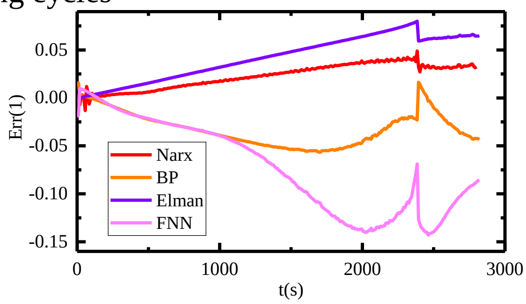

(c2) Estimated error without EKF optimization

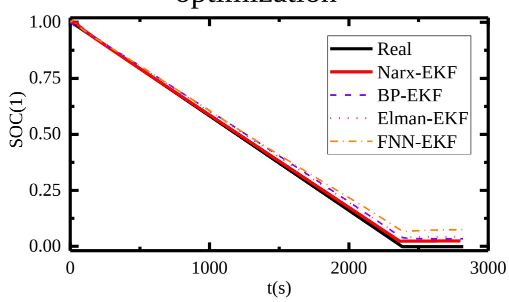

(c3) SOC estimation optimized by EKF

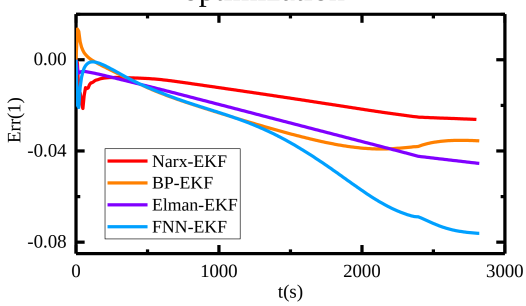

(c4) Estimated error optimized by EKF

(c) 126 aging cycles

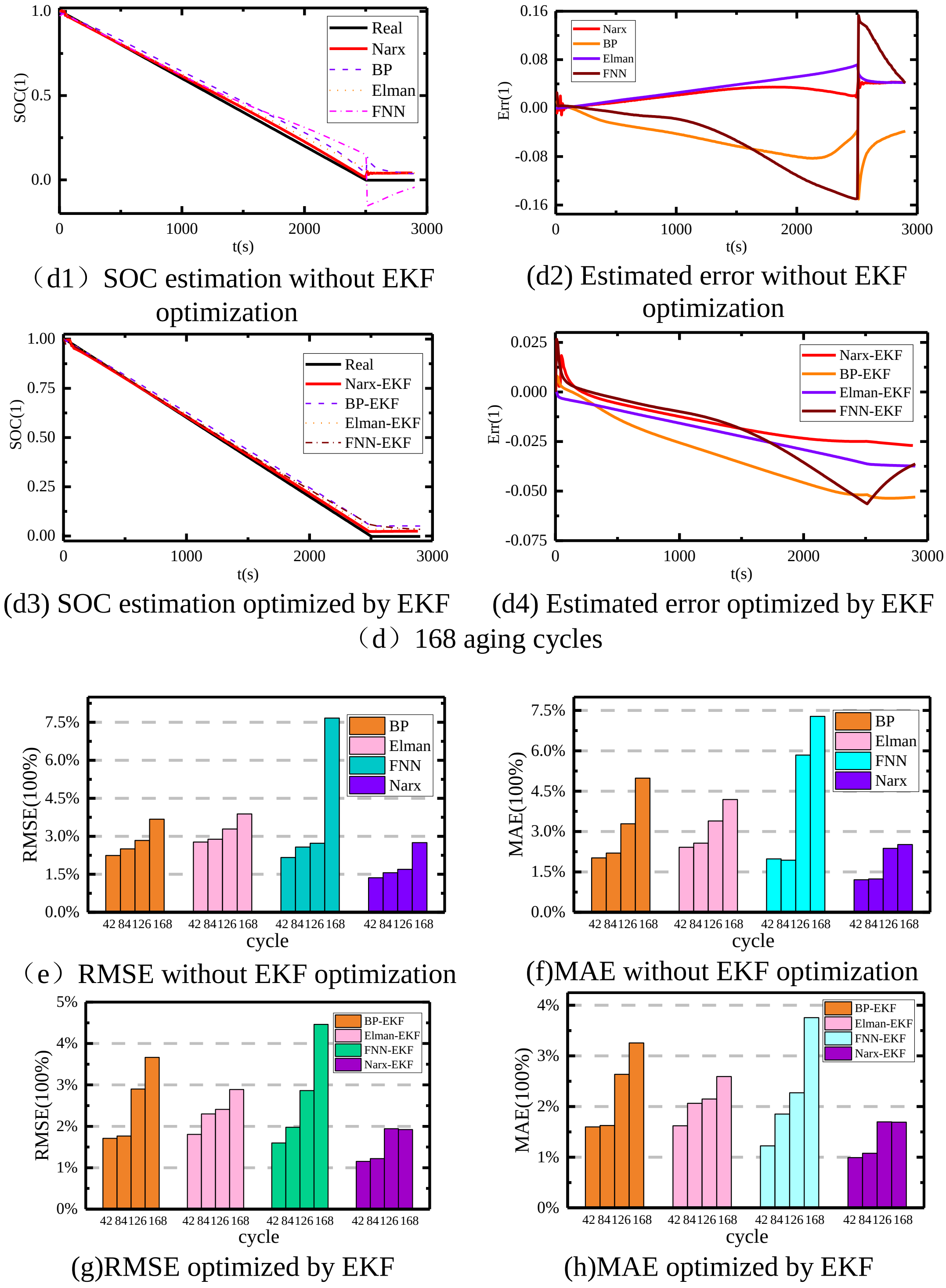

Figure 12. Simulation test under different aging cycles

As shown in the figure above, it can be seen from (a), (b), (c) and (d) that, at each aging stage, the NARXNN has higher accuracy and robustness than other neural networks. After EKF optimization, the accuracy and convergence effect of each algorithm is dramatically improved. From (e), (f), (g), and (h), it can be seen that the RMSE and MAE of the NARXNN are 1.4% and 1.2% under 42 aging cycles. After 82 aging cycles, the accuracy of the SOC decreases, and the RMSE and MAE are 1.6% and 1.2%, respectively. When the battery is deeply cycled, the SOC accuracy will further decrease. After 168 aging cycles, the RMSE and MAE reached 2.7% and 2.5% respectively. However, under all aging cycle conditions, the SOC error remains below ±5%. After EKF optimization, the MAE and RMSE of all algorithms are significantly reduced. The RMSE and MAE of NARX-EKF are reduced by about 30% relative to NARXNN. In addition, compared with the GPR model, the model proposed in this study has greater advantages. The GPR was validated through experiments and obtained SOC error under 6% under different dynamic profiles and aging cycles[39]. It can be seen that the NARX-EKF network can well solve the impact of different degrees of aging of lithium-ion batteries on SOC estimation.

4. CONCLUSIONS

This paper presents a method for estimating the SOC of lithium-ion batteries based on the NARX-EKF neural network. In selecting the dataset, the data under different working conditions are used as the network's training set and test set, including DST working condition, BBDST working condition, cyclic charge and discharge working condition, and data under different aging cycles. Experimental results show that the open-loop NARXNN structure is suitable for cyclic operating conditions. The maximum error of NARXNN is about 2.5%, which is smaller than other neural networks. RMSE and MAE are only 1.4% and 1.3% respectively, much lower than other neural networks. The NARXNN can follow the reference value stably for dynamic working conditions, and the error is maintained within 4%, which is much lower than other neural networks. The NARXNN optimized by EKF reduces the maximum error from 4% to 2.2%. The accuracy is increased by 80%, which shows that the NARX-EKF network has high accuracy in battery SOC estimation. Considering the influence of ambient temperature, a NARXNN is constructed for narrow temperature changes. The experimental results show the estimation advantage of NARXNN. Under low-temperature conditions, its RMSE and MAE are 1.2% and 0.9%, respectively. Under high-temperature conditions, the RMSE and MAE are 0.6% and 0.5%, respectively. After EKF optimization, both the RMSE and MAE are significantly reduced regardless of high temperature or low-temperature conditions. In addition, under different aging cycle tests, the SOC error is kept within ±5%, which is far better than other neural networks. After EKF optimization, the RMSE and MAE of the NARX-EKF are reduced by about 30% relative to NARXNN. Compared with traditional model-based estimation methods, this method is completely driven by data and is not limited by battery materials or models. Therefore, it can be easily applied to battery management systems of different types and scenarios for the accurate estimation of SOC.

ACKNOWLEDGMENTS
The work was supported by National Natural Science Foundation of China (No. 61801407).

References

1. M. A. Hannan, M. M. Hoque, A. Hussain, Y. Yusof and P. J. Ker, *Ieee Access*, 6 (2018) 19362.
2. E. Pomerantseva, F. Bonaccorso, X. L. Feng, Y. Cui and Y. Gogotsi, *Science*, 366 (2019) 969.

3. H. L. Zhang, J. K. Peng, H. C. Tan, H. X. Dong, F. Ding and B. Ran, *Applied Energy*, 269 (2020) 768.
4. Z. X. Tan, X. R. Li, L. He, Y. Li and J. Y. Huang, *Int J Elec Power*, 117 (2020) 2014.
5. H. L. Wang, G. B. Zhou, R. Xue, Y. J. Lu and J. A. McCann, *Ieee T Intell Transp*, 21 (2020) 2090.
6. Z. H. Huang, C. P. Zhao, H. Li, W. Peng, Z. Zhang and Q. S. Wang, *Energy*, 205 (2020) 542.
7. X. S. Hu, H. F. Jiang, F. Feng and B. Liu, *Applied Energy*, 257 (2020) 445.
8. H. Myneni and S. K. Ganjikunta, *Ieee T Sustain Energ*, 11 (2020) 1739.
9. B. B. Mao, H. D. Chen, L. Jiang, C. P. Zhao, J. H. Sun and Q. S. Wang, *Process Saf Environ*, 139 (2020) 133.
10. B. Jiang, H. F. Dai and X. Z. Wei, *Applied Energy*, 269 (2020) 425.
11. S. M. Peng, X. L. Zhu, Y. J. Xing, H. B. Shi, X. Cai and M. Pecht, *J Power Sources*, 392 (2018) 48.
12. G. Thenaisie, C. H. Park, J. H. Cho and S. G. Lee, *Measurement*, 158 (2020) 1243.
13. R. Xiong, J. Y. Cao, Q. Q. Yu, H. W. He and F. C. Sun, *Ieee Access*, 6 (2018) 1832.
14. S. Ullah, L. Khan, R. Badar, A. Ullah, F. W. Karam, Z. A. Khan and A. U. Rehman, *Plos One*, 15 (2020) 4576.
15. R. Xiong, L. L. Li, Q. Q. Yu, Q. Jin and R. X. Yang, *Journal of Cleaner Production*, 249 (2020) 1764.
16. Z. Y. Song, H. Wang, J. Hou, H. F. Hofmann and J. Sun, *Ieee T Power Electr*, 35 (2020) 4439.
17. C. Zhang, W. Allafi, Q. Dinh, P. Ascencio and J. Marco, *Energy*, 142 (2018) 678.
18. S. H. Wang, Y. Yang and K. H. Guo, *Mathematical Problems in Engineering*, 2020 (2020)789.
19. L. He, M. K. Hu, Y. J. Wei, B. J. Liu and Q. Shi, *Sci China Technol Sc*, 63 (2020) 410.
20. S. L. Wang, C. Fernandez, W. Cao, C. Y. Zou, C. M. Yu and X. X. Li, *J Power Sources*, 428 (2019) 67.
21. S. Li, K. Li, E. Xiao and C. K. Wong, *Ieee T Ind Electron*, 67 (2020) 8484.
22. C. F. Yang, X. Y. Wang, Q. H. Fang, H. F. Dai, Y. Q. Cao and X. Z. Wei, *Journal of Energy Storage*, 29 (2020) 897.
23. X. H. Qiu, W. X. Wu and S. F. Wang, *J Power Sources*, 450 (2020) 364.
24. Z. M. Xi, M. Dahmardeh, B. Xia, Y. H. Fu and C. Mi, *Ieee T Veh Technol*, 68 (2019) 8613.
25. Y. Ma, Y. Chen, X. W. Zhou and H. Chen, *Ieee T Contr Syst T*, 27 (2019) 1788.
26. S. L. Wang, C. Fernandez, Y. C. Fan, J. Q. Feng, C. M. Yu, K. F. Huang and W. Xie, *Energy Science & Engineering*, 8 (2020) 1484.
27. D. T. Liu, L. Li, Y. C. Song, L. F. Wu and Y. Peng, *Int J Elec Power*, 110 (2019) 48.
28. M. Jiao, D. Q. Wang and J. L. Qiu, *J Power Sources*, 459 (2020) 748.
29. D. J. Xuan, Z. F. Shi, J. Z. Chen, C. Y. Zhang and Y. X. Wang, *Journal of Cleaner Production*, 252 (2020) 8764.
30. J. K. Peng, J. Y. Luo, H. W. He and B. Lu, *Applied Energy*, 253 (2019) 4687.
31. B. Jiang, H. F. Dai, X. Z. Wei and T. J. Xu, *Applied Energy*, 253 (2019) 568.
32. S. L. Wang, C. Fernandez, L. P. Shang, Z. F. Li and J. C. Li, *Journal of Energy Storage*, 9 (2017) 69.
33. X. Zhang, Y. J. Wang, D. Yang and Z. H. Chen, *Energy*, 115 (2016) 219.
34. R. Xiong, Y. Z. Zhang, H. W. He, X. Zhou and M. G. Pecht, *Ieee T Ind Electron*, 65 (2018) 1526.
35. F. Lotfi, S. Ziapour, F. Faraji and H. D. Taghirad, *Int J Elec Power*, 117 (2020) 1236.
36. D.-J. Xuan, Z. Shi, J. Chen, C. Zhang and Y.-X. Wang, *Journal of Cleaner Production*, (2019) 5987.
37. B. Haus and P. Mercorelli, *Ieee T Veh Technol*, 69 (2020) 1452.
38. M. Lucu, E. Martinez-Laserna, I. Gandiaga, K. Liu, H. Camblong, W. D. Widanage and J. Marco, *Journal of Energy Storage*, 30 (2020) 4251.

39. S. Z. Zhang, G. Xu, X. X. Dou and X. W. Zhang, *Sustain Energy Techn*, 40 (2020) 45.
40. A. H. Ran, Z. H. Zhou, S. X. Chen, P. B. Nie, K. Qian, Z. L. Li, B. H. Li, H. B. Sun, F. Y. Kang, X. Zhang and G. D. Wei, *Adv Theor Simul*, 3 (2020) 985.
41. S. Korneev, H. Arunachalam, S. Onori and I. Battiato, *Transport Porous Med*, 134 (2020) 173.
42. S. S. Sheikh, M. Anjum, M. A. Khan, S. A. Hassan, H. A. Khalid, A. Gastli and L. Ben-Brahim, *Energies*, 13 (2020) 697.
43. E. Chemali, P. J. Kollmeyer, M. Preindl and A. Emadi, *J Power Sources*, 400 (2018) 242.